A PHYSICAL MODEL OF THE TROMBONE USING DYNAMIC GRIDS FOR FINITE DIFFERENCE SCHEMES

Silvin Willemsen
Multisensory Experience Lab
Aalborg University Copenhagen
Copenhagen, Denmark
sil@create.aau.dk

Stefan Bilbao, Michele Ducceschi
Acoustics and Audio Group
University of Edinburgh
Edinburgh, UK

Stefania Serafin
Multisensory Experience Lab
Aalborg University Copenhagen
Copenhagen, Denmark

ABSTRACT

We propose a complete simulation of a trombone based on finite difference schemes (FDSs). In particular, we propose a novel method to dynamically vary the number of grid points in the grid, to simulate the fact that that physical dimension of the trombone's resonator dynamically varies over time. We describe the different elements of the model and present the results of our simulations.

1. INTRODUCTION

The trombone is a musical instrument which is interesting to simulate from different viewpoints. From the point of view of the excitation, the interaction between the lips and the player has been extensively studied, and simulated mostly using a simple mass-spring damper system [1]. The sound propagation in the trombone also presents some very interesting nonlinearities, which have been investigated and simulated [1, 2, 3]. One of the interesting characteristics of this instrument is the fact that the physical dimensions of the resonator vary while playing it. Some synthesis techniques such as digital waveguides allow to approach the issue of dynamic resonator changes in a simple and computationally efficient way, and this feature has been extensively used in real-time sound synthesis [4].

However, when modelling the resonator of the instrument using finite-difference time-domain (FDTD) methods, or finite difference schemes (FDSs), the issue is not as trivial, and changes might compromise stability. Previous implementations of brass instruments using FDSs focus on the trumpet [5]. To our knowledge, the simulation of a trombone varying the shape of the resonator in real time using FDSs has not been addressed yet. We can cope with this limitation by having a grid that dynamically changes while the simulation is running as shown in a companion paper [6].

Briefly described, we modify the grid configurations of the FDS by adding and subtracting grid points based on parameters describing the system. In this paper we propose a full simulation of a trombone, describing all its elements in detail with a specific focus on the dynamic grid simulation.

This paper is structured as follows: Section 2 presents the models for the tube and lip reed in continuous time. Section 3 briefly introduces FDTD methods and then discretises the aforementioned continuous equations. Section 4 presents the dynamic grid used to simulate the trombone slide and details on the implementation are provided in Section 5. Section 6 presents the results of the simulation, and finally, some conclusory remarks appear in Section 7.

2. CONTINUOUS SYSTEM

Wave propagation in an acoustic tube can be approximated using a 1-dimensional model. Consider a tube of time-varying length $L = L(t)$ (in m) defined over spatial domain $x \in [0, L]$ and time $t \geq 0$. Using operators ∂_t and ∂_x denoting a first-order derivative with respect to time t and space x, respectively, a system of first-order PDEs describing the wave propagation in an acoustic tube can then be written as

$$\frac{S}{\rho_0 c^2}\partial_t p = -\partial_x(Sv) \tag{1a}$$

$$\rho_0 \partial_t v = -\partial_x p \tag{1b}$$

with pressure $p = p(x,t)$ (in N/m^2), particle velocity $v = v(x,t)$ (in m/s) and (circular) cross-sectional area $S(x)$ (in m^2). Furthermore, ρ_0 is the density of air (in kg/m^3) and c is the speed of sound in air (in m/s).

Boundary conditions can then be imposed at the ends of domain, $x = 0, L$. We assume the left boundary (at the mouthpiece) to be closed and the right (at the bell) to be open according to

$$S(0,t)v(0,t) = 0, \quad \text{(Neumann, closed)} \tag{2a}$$

$$p(L,t) = 0. \quad \text{(Dirichlet, open)} \tag{2b}$$

In the following, these (lossless) boundary conditions will be modified to be coupled to a lip reed and radiating respectively.

2.1. Coupling to a Lip Reed

To excite the system, a lip reed can be modelled as a simple mass-spring-damper system. In the following, y can be seen as the moving the upper lip where the lower lip is left static and rigid. See Figure 1 for a full schematic of the lip reed model. Using dots to indicate time-derivatives the lip reed is modelled as

$$M_\mathrm{r}\ddot{y} = -M_\mathrm{r}\omega_0^2 y - M_\mathrm{r}\sigma_\mathrm{r}\dot{y} + \psi(\dot{\psi}/\dot{\eta}) + S_\mathrm{r}\Delta p, \tag{3}$$

with displacement from the equilibrium $y = y(t)$, lip mass M_r (in kg), externally supplied (angular) frequency of oscillation $w_0 = w_0(t) = \sqrt{K_\mathrm{r}/M_\mathrm{r}}$ (in rad/s) and stiffness $K = K(t)$ (in N/m).

We extend the existing models of lip reeds [1] by introducing a nonlinear collision between the lips based on potential quadrati-

sation proposed by [7]. The collision potential is defined as

$$\psi = \left(\frac{2K_\mathrm{c}}{\alpha_\mathrm{c}+1} [\eta]_+^{\alpha_\mathrm{c}+1} \right)^{1/2} \tag{4}$$

$$K_\mathrm{c} > 0, \quad \alpha_\mathrm{c} \geq 1, \quad \eta \triangleq -y - H_0$$

with collision stiffness K_c (in N/m if $\alpha_\mathrm{c} = 1$) dimensionless nonlinear collision coefficient α_c, inverted distance between the lips $\eta = \eta(t)$ (in m), $[\eta]_+ = 0.5(\eta + |\eta|)$ describing the "positive part of η", and static equilibrium separation H_0 (in m). Notice, that if $\eta \leq 0$ the collision potential will be non-zero. This quadratic form of a collision potential allows for an non-iterative implementation [7]. This will be elaborated on in Section 3.

Finally, S_r (in m^2) is the effective surface area and

$$\Delta p = P_\mathrm{m} - p(0,t) \tag{5}$$

is the difference between the externally supplied pressure in the mouth $P_\mathrm{m} = P_\mathrm{m}(t)$ and the pressure in the mouth piece $p(0,t)$ (all in Pa). This pressure difference causes a volume flow velocity following the Bernoulli equation

$$U_\mathrm{B} = w_\mathrm{r}[-\eta]_+ \mathrm{sgn}(\Delta p) \sqrt{\frac{2|\Delta p|}{\rho_0}}, \tag{6}$$

(in m/s) with effective lip-reed width w_r (m). Notice that when $\eta \geq 0$, the lips are closed and the volume velocity U_B is 0. Another volume flow is generated by the lip reed itself according to

$$U_\mathrm{r} = S_\mathrm{r} \frac{dy}{dt} \tag{7}$$

(in m/s). Assuming that the volume flow velocity is conserved, the total air volume entering the system is defined as

$$S(0)v(0,t) = U_\mathrm{B}(t) + U_\mathrm{r}(t). \tag{8}$$

The lip reed can then be coupled to the tube by modifying boundary condition (2a) to (8).

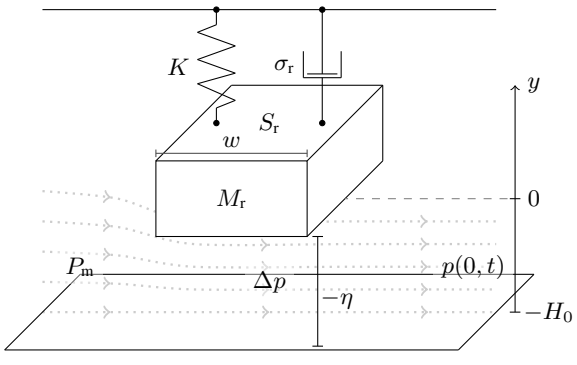

Figure 1: Lipsystem with the equilibrium at 0 and the distance from the lower lip H_0. The various symbols relate to those used in Eq. (3).

2.2. Radiation

As the bell-end of brass instruments is in a way "coupled" to the air, the tube loses energy at the bell, or right boundary. These losses can be modelled using a radiation model and lossless condition (2b) can be modified to be radiating instead. The radiation model used is the one for the unflanged cylindrical pipe proposed by Levine and Schwinger in [8] and discretised by Silva *et al.* in [9]. As this model is not important for the contribution of this work it will not be detailed here in full. The interested reader is instead referred to [10] for a comprehensive explanation.

3. DISCRETISATION

The continuous system described in the previous section is discretised using FDTD methods, which subdivide continuous equations into discrete points in space and time. Before moving on to this discretisation, we briefly introduce these methods along with several finite-difference operators.

3.1. Numerical Methods

Consider a 1D system described by state variable $u = u(x,t)$ with spatial domain $x \in \mathbb{R}$ and time $t \geq 0$. The spatial domain can be disctretised according to $x = lh$ with spatial index $l \in \mathbb{Z}$ and grid spacing h (in m) and time as $t = nk$ with temporal index $n \in \mathbb{Z}^{0+}$ and time step k (in s). Using these discrete variables state variable $u(x,t)$ can be discretised to grid function u_l^n.

Shift operators can then be applied to grid function u_l^n. Temporal and spatial shift operators are

$$\begin{aligned} e_{t+}u_l^n &= u_l^{n+1}, \quad e_{t-}u_l^n = u_l^{n-1}, \\ e_{x+}u_l^n &= u_{l+1}^n, \quad e_{x-}u_l^n = u_{l-1}^n, \end{aligned} \tag{9}$$

from which more complex operators can be derived. First-order derivatives can be approximated using forward, backward and centred difference operators in time

$$\delta_{t+} = \frac{e_{t+} - 1}{k}, \; \delta_{t-} = \frac{1 - e_{t-}}{k}, \; \delta_{t\cdot} = \frac{e_{t+} - e_{t-}}{2k}, \tag{10}$$

(all approximating ∂_t) and space

$$\delta_{x+} = \frac{e_{x+} - 1}{h}, \; \delta_{x-} = \frac{1 - e_{x-}}{h}, \; \delta_{x\cdot} = \frac{e_{x+} - e_{x-}}{2h}, \tag{11}$$

(all approximating ∂_x) where the identity operator 1 does not introduce any shift.

Furthermore, forward, backward and centred averaging operators can be defined in time

$$\mu_{t+} = \frac{e_{t+} + 1}{2}, \; \mu_{t-} = \frac{1 + e_{t-}}{2}, \; \mu_{t\cdot} = \frac{e_{t+} + e_{t-}}{2}, \tag{12}$$

and space

$$\mu_{x+} = \frac{e_{x+} + 1}{2}, \; \mu_{x-} = \frac{1 + e_{x-}}{2}, \; \mu_{x\cdot} = \frac{e_{x+} + e_{x-}}{2}. \tag{13}$$

Here, forward and backward averaging operators are extremely useful in the context of first-order systems as used in this paper. When applied to a grid function, the result may be interpreted as

its value shifted by half a temporal or spatial step:

$$\mu_{t+}u_l^n = u_l^{n+1/2}, \quad \mu_{t-}u_l^n = u_l^{n-1/2}, \tag{14}$$

$$\mu_{x+}u_l^n = u_{l+1/2}^n, \quad \mu_{x-}u_l^n = u_{l-1/2}^n, \tag{15}$$

effectively placing the grid function on an *interleaved grid* which will be further elaborated on in the following.

3.2. Discrete Tube

We start discretising system (1) by placing velocity v on an interleaved grid, following [10], both in space and time. Domain $x \in [0, L]$ can be discretised to $l = [0, \ldots, N]$ where number of intervals between grid points is calculated using (same issue here as in the other paper)

$$N = \lfloor L/h \rfloor. \tag{16}$$

The grid functions $p_l^n \approx p(x,t)$ and $v_{l+1/2}^{n+1/2} \approx v(x,t)$ (with reduced domain $l = [0, \ldots, N-1]$) with $N+1$ and N grid points respectively are then introduced along with discrete cross-sectional area $S_l \approx S(x)$ sampled at $x = lh$ to which the spatial operators defined in Section 3.1 can also be applied.

System (1) can then be discretised into the following system of FDSs

$$\frac{\bar{S}_l}{\rho_0 c^2}\delta_{t+}p_l^n = -\delta_{x-}(S_{l+1/2}v_{l+1/2}^{n+1/2}), \tag{17a}$$

$$\rho_0 \delta_{t-}v_{l+1/2}^{n+1/2} = -\delta_{x+}p_l^n, \tag{17b}$$

where $S_{l+1/2} = \mu_{x+}S_l$ and $\bar{S}_l = \mu_{x-}S_{l+1/2}$ are approximations to the continuous cross-sectional area $S(x)$. The values for $\bar{S}_l$ at the boundaries, i.e., $\bar{S}_0$ and $\bar{S}_N$ are set equal to $S(0)$ and $S(L)$.

Expanding the operators, we obtain the following recursion

$$p_l^{n+1} = p_l^n - \frac{\rho_0 c\lambda}{\bar{S}_l}(S_{l+1/2}v_{l+1/2}^{n+1/2} - S_{l-1/2}v_{l-1/2}^{n+1/2}), \tag{18a}$$

$$v_{l+1/2}^{n+1/2} = v_{l+1/2}^{n-1/2} - \frac{\lambda}{\rho_0 c}(p_{l+1}^n - p_l^n), \tag{18b}$$

where $\lambda = ck/h$ is referred to as the Courant number and

$$\lambda \leq 1 \tag{19}$$

in order for the scheme to be stable.

Finally, the boundary conditions in (2) can be discretised as

$$\mu_{x-}\left(S_{1/2}v_{1/2}^{n+1/2}\right) = 0 \tag{20a}$$

$$p_N^n = 0 \tag{20b}$$

3.3. Lip reed

As the lip reed interacts with the particle velocity of the tube, it is placed on the interleaved temporal grid, but kept on the regular spatial grid, as it interacts with the boundary at $l = 0$.

Equations (3) - (8) are discretised as follows:

$$\begin{aligned} M_{\mathrm{r}}\delta_{tt}y^{n+1/2} = &- M_{\mathrm{r}}\omega_0^2\mu_{t\cdot}y^{n+1/2} - M_{\mathrm{r}}\sigma_{\mathrm{r}}\delta_{t\cdot}y^{n+1/2} \\ &+ (\mu_{t+}\psi^n)\, g^{n+1/2} + S_{\mathrm{r}}\Delta p^{n+1/2}, \end{aligned} \tag{21a}$$

$$\Delta p^{n+1/2} = P_{\mathrm{m}} - \mu_{t+}p_0^n, \tag{21b}$$

$$\begin{aligned} U_{\mathrm{B}}^{n+1/2} = &\, w_{\mathrm{r}}[-\eta^{n+1/2}]_+ \mathrm{sgn}(\Delta p^{n+1/2}) \\ &\cdot \sqrt{2|\Delta p^{n+1/2}|/\rho_0}, \end{aligned} \tag{21c}$$

$$U_{\mathrm{r}}^{n+1/2} = S_{\mathrm{r}}\delta_{t\cdot}y^{n+1/2}, \tag{21d}$$

$$\mu_{x-}(S_{1/2}v_{1/2}^{n+1/2}) = U_{\mathrm{B}}^{n+1/2} + U_{\mathrm{r}}^{n+1/2}, \tag{21e}$$

where $\omega_0 = \omega_0^{n+1/2}$ and $P_{\mathrm{m}} = P_{\mathrm{m}}^{n+1/2}$ and

$$g^{n+1/2} = \begin{cases} \kappa\sqrt{\dfrac{K_{\mathrm{c}}(\alpha+1)}{2}} & \\ \quad \cdot (\eta^{n+1/2})^{\frac{\alpha-1}{2}} & \text{if } \eta^{n+1/2} \geq 0 \quad (22a) \\ -2\dfrac{\psi^n}{\eta^\star - \eta^{n-1/2}} & \text{if } \eta^{n+1/2} < 0 \quad (22b) \end{cases}$$

and $\kappa = 1$ if $\psi^n \geq 0$, otherwise $\kappa = -1$. Finally, $\eta^\star = -y^\star - H_0$ where $y^\star$ is the value of $y^{n+3/2}$ calculated using system (21) (after expansion) without the collision potential. This means that system (21) needs to be calculated twice every iteration, once without the collision term and once with. The process of calculating the pressure difference $\Delta p^{n+1/2}$ in (21) will not be given here, but the interested reader is referred to [10, Ch. 5] for a derivation.

Finally, to couple the lip reed to the tube, boundary condition (20a) can be modified to Eq. (21e).

4. DYNAMIC GRID

Arguably the most characteristic feature of the trombone is its slide with which the length of the tube is altered and the resonating frequencies are changed. In a companion article [6], we present a method to dynamically change grid configurations of FDSs by adding and subtracting grid points based on paramters describing the system. Though [6] shows changes in the wavespeed c rather than the length L, the effect of a change in either of these parameters has an identical effect on these systems as long as the geometry is unchanged for the grid points. Leaving c fixed also means that grid spacing h does not change during the simulation, but rather the spatial domain of the system. Note that this method only works for slow (sub-audio rate) parameter changes.

We can split a tube with time-varying length L^n into two smaller sections with lengths L_p^n and L_q^n (in m) such that $L^n = L_p^n + L_q^n$. Splitting the FDSs in (17) in this way yields two sets of first-order systems. The pressure and particle velocity of the first (left) system $p_{l_p}^n$ and $v_{l_p+1/2}^{n+1/2}$ are both defined over discrete domain $l_p = [0, \ldots, M^n]$, and those of the second (right) system $q_{l_q}^n$ and $w_{l_q-1/2}^{n+1/2}$ are defined over discrete domain $l_q = [0, \ldots, M_q^n]$, with

$$M^n = \lceil L_p^n/h \rceil, \quad \text{and} \quad M_q^n = \lfloor L_q^n/h \rfloor \tag{23}$$

where $\lceil\cdot\rceil$ and $\lfloor\cdot\rfloor$ denote the ceiling and flooring operation respectively. Note, that the domains for v and w have an extra grid point when compared to the regular case in (17) and that w is indexed with $l_q - 1/2$ rather than $l_q + 1/2$. The resulting system of FDSs

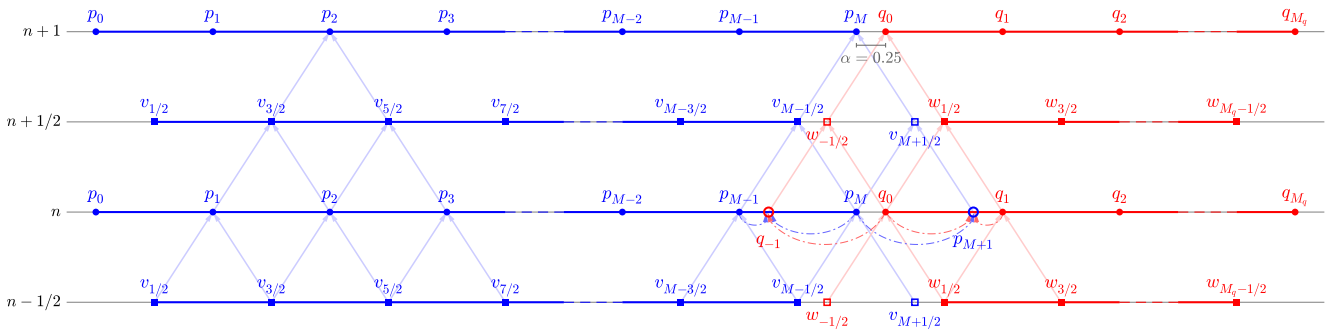

Figure 2: Schematic showing data flow of how different grid points at time index $n+1$ are calculated with $\alpha = 0.25$ in Eq. (27). To prevent cluttering, arrows going straight up (indicating that the state of a grid point at time step n is needed to calculate the state of that grid point at $n+1$) are suppressed. As an example of the usual case, the points required to calculate p_2^{n+1} are shown (refer to Eq. (18)). Furthermore, the points needed to calculate p_M^{n+1} and q_0^{n+1} are shown. The most important difference with the usual case is that the virtual grid points $p_{M_p+1}^n$ and q_{-1}^n are the result of the interpolation of known pressure values at n using Eq. (29).

then becomes

$$\frac{\bar{S}_l}{\rho_0 c^2}\delta_{t+} p_{l_p}^n = -\delta_{x-}(S_{l+1/2} v_{l_p+1/2}^{n+1/2}), \tag{24a}$$

$$\rho_0 \delta_{t-} v_{l_p+1/2}^{n+1/2} = -\delta_{x+} p_{l_p}^n, \tag{24b}$$

$$\frac{\bar{S}_l}{\rho_0 c^2}\delta_{t+} q_{l_q}^n = -\delta_{x+}(S_{l-1/2} w_{l_q-1/2}^{n+1/2}), \tag{24c}$$

$$\rho_0 \delta_{t-} w_{l_q-1/2}^{n+1/2} = -\delta_{x-} q_{l_q}^n. \tag{24d}$$

Here, due to the different indexing for w, the spatial derivatives for the right system are flipped. Also note, that l is still used for the spatial indices of $\bar{S}$ and S, where $l \in [l_p, l_q + M^n]$. The conditions for the outer boundaries of this system, i.e., at $l_p = 0$ and $l_q = M_q^n$, are the same as for the full system. The inner boundaries, $l_p = M^n$ and $l_q = 0$ are connected according to the method described in [6] which will be explained shortly. To be able to calculate p_M^{n+1} and q_0^{n+1}, the domains of v and w have been extended at the inner boundaries to include $v_{M+1/2}^{n+1/2}$ and $w_{-1/2}^{n+1/2}$. These, however, need points outside of the domains of $p_{l_p}^n$ and $q_{l_q}^n$, i.e., p_{M+1}^n and q_{-1}^n. In [6] we propose to calculate these *virtual grid points* based on known values of the system. Despite the fact that [6] presents the method using a second-order system, it can still be applied here. The process of how the p_M^{n+1} and q_0^{n+1} are calculated is visualised in in Figure 2.

4.1. Changing the Tube Length

In the following, the location of a grid point u_l along the grid (in m from the left boundary) from is denoted as x_{u_l}.

The two pairs of first order systems in (24) are placed on the same domain x with

$$x_{p_{l_p}} = l_p h, \quad \text{and} \quad x_{q_{l_q}} = L^n - (M_q^n - l_q)h \tag{25}$$

describing the locations of the left system and right system respectively. It can be observed from Eq. (25) that as the tube length L^n changes, the locations of the grid points of the right system will change. More specifically, as the trombone-slide is extended and L^n increases, all grid points of the right system move to the right, and vice versa for a contracting slide. If L^n is changed in a smooth fashion, the continuous domain $x \in [0, L^n]$ will not necessarily be subdivided into an integer amount of intervals N^n (of size h). This is where a *fractional* number of intervals is introduced and is defined as

$$\mathcal{N}^n = L^n/h, \tag{26}$$

which is essentially Eq. (16) without the flooring operation, and $N^n = \lfloor \mathcal{N}^n \rfloor$. The fractional part of $\mathcal{N}^n$ can then be calculated using

$$\alpha = \alpha^n = \mathcal{N}^n - N^n, \tag{27}$$

which describes the distance between the inner boundaries along the grid in terms of how many times h would fit in-between (which is always less than once). If $\mathcal{N}^n = N^n$ and $\alpha = 0$, the inner boundaries p_M and q_0 perfectly overlap, i.e., $x_{p_M}^n = x_{q_0}^n$. This also means that the domain x can be exactly divided into N^n equal intervals of size h. As the virtual grid points p_{M+1}^n and q_{-1}^n perfectly overlap with q_1^n and p_{M-1}^n respectively, these values can be used directly to calculate the inner boundaries. This situation effectively acts as a rigid connection between the inner boundaries defined as

$$p_M^n = q_0^n. \tag{28}$$

If $\alpha \neq 0$, some other definition for p_{M+1}^n and q_{-1}^n needs to be found. We use quadratic Lagrangian interpolation according to

$$p_{M+1}^n = \frac{\alpha - 1}{\alpha + 1} p_M^n + q_0^n - \frac{\alpha - 1}{\alpha + 1} q_1^n \tag{29a}$$

$$q_{-1}^n = -\frac{\alpha - 1}{\alpha + 1} p_{M-1}^n + p_M^n + \frac{\alpha - 1}{\alpha + 1} q_0^n. \tag{29b}$$

which can then be used to calculate $v_{M+1/2}^{n+1/2}$ and $w_{-1/2}^{n+1/2}$ and consequently p_M^{n+1} and q_0^{n+1}. This process repeats every sample. It can be shown through the rigid connection in (28), that if $\alpha = 0$, the definitions in (29) reduce to $p_{M+1}^n = q_1^n$ and $q_{-1}^n = p_{M-1}^n$ as stated before.

4.2. Adding and removing grid points

As the tube length L^n changes, L_p^n and L_q^n also change according to

$$L_p^n = L_p^{n-1} + 0.5L_{\text{diff}}^n, \quad L_q^n = L_q^{n-1} + 0.5L_{\text{diff}}^n, \tag{30}$$

where

$$L_{\text{diff}}^n = L^n - L^{n-1}, \tag{31}$$

which causes the number of points M^n and M_q^n to change as well according to Eq. (23). The following state vectors are introduced for the pressure, defined for $n+1$ and n

$$\mathbf{p}^n = [p_0^n, p_1^n, ..., p_M^n]^T, \ \mathbf{q}^n = [q_0^n, q_1^n, ..., q_{M_q}^n]^T \tag{32}$$

and for the velocity, defined for $n+1/2$ and $n-1/2$

$$\begin{aligned} \mathbf{v}^{n-1/2} &= [v_{1/2}^{n-1/2}, v_{3/2}^{n-1/2}, ..., v_{M+1/2}^{n-1/2}]^T \\ \mathbf{w}^{n-1/2} &= [w_{-1/2}^{n-1/2}, w_{1/2}^{n-1/2}, ..., w_{M_q-1/2}^{n-1/2}]^T \end{aligned} \tag{33}$$

and contain the different states over the discrete domains defined at the beginning of this section. Here, T denotes the transpose operation.

If $N^n > N^{n-1}$, points are added to the left and right system in an alternating fashion ($n-1$ is used later on for the state correction, say something about that here or leave for Section 5.3..?)

$$\begin{cases} \mathbf{p}^n = [(\mathbf{p}^n)^T, I_3\mathbf{r}^n]^T \\ \mathbf{v}^{n-1/2} = [(\mathbf{v}^{n-1/2})^T, I_3\mathbf{z}_v^{n-1/2}]^T \end{cases} \text{if } N^n \text{ is odd,}$$
$$\begin{cases} \mathbf{q}^n = [I_3^{\leftarrow}\mathbf{r}^n, (\mathbf{q}^n)^T]^T \\ \mathbf{w}^{n-1/2} = [I_3^{\leftarrow}\mathbf{z}_w^{n-1/2}, (\mathbf{w}^{n-1/2})^T]^T \end{cases} \text{if } N^n \text{ is even,} \tag{34}$$

where

$$\begin{aligned} \mathbf{r}^n &= [p_{M-1}^n, p_M^n, q_0^n, q_1^n]^T, \\ \mathbf{z}_v^{n-1/2} &= [v_{M-1/2}^{n-1/2}, v_{M+1/2}^{n-1/2}, w_{1/2}^{n-1/2}, w_{3/2}^{n-1/2}]^T - \boldsymbol{\eta}, \\ \mathbf{z}_w^{n-1/2} &= [v_{M-3/2}^{n-1/2}, v_{M-1/2}^{n-1/2}, w_{-1/2}^{n-1/2}, w_{1/2}^{n-1/2}]^T + \boldsymbol{\eta}^{\leftarrow}, \end{aligned} \tag{35}$$

cubic Lagrangian interpolator

$$I_3 = \left[-\tfrac{\alpha(\alpha+1)}{(\alpha+2)(\alpha+3)} \quad \tfrac{2\alpha}{\alpha+2} \quad \tfrac{2}{\alpha+2} \quad -\tfrac{2\alpha}{(\alpha+3)(\alpha+2)}\right], \tag{36}$$

and

$$\boldsymbol{\eta} = \boldsymbol{\eta}^{n-1/2} = \left(w_{-1/2}^{n-1/2} - v_{M+1/2}^{n-1/2}\right) \cdot [0, 0, 1, 1]^T \tag{37}$$

adds an offset to half of the $\mathbf{z}$ vectors depending on the state-difference between the inner boundaries of v and w. This will be further explained in Section 4.3. Finally, $I_3^{\leftarrow}$ and $\boldsymbol{\eta}^{\leftarrow}$ are flipped versions of (36) and (37) respectively.

If $N^n < N^{n-1}$ points are simply removed from the vectors according to

$$\begin{cases} \mathbf{p}^n = [p_0^n, \dots, p_{M-1}^n]^T \\ \mathbf{v}^{n-1/2} = [v_{1/2}^{n-1/2}, \dots, v_{M-1/2}^{n-1/2}]^T \end{cases} \text{if } N^n \text{ is even,}$$
$$\begin{cases} \mathbf{q}^n = [q_1^n, \dots, q_{M_q}^n]^T \\ \mathbf{w}^{n-1/2} = [w_{1/2}^{n-1/2}, \dots, w_{M_q-1/2}^{n-1/2}]^T \end{cases} \text{if } N^n \text{ is odd,} \tag{38}$$

4.3. Drift of w

The inner boundaries of the pressure states p and q are connected by (29), but no such connection exists for the velocity states v and w. As this leaves w without any boundary condition (recall that the right boundary condition only exists for the pressure as in (20b)) it is only "held in place" by the pressure values of q, or more specifically, by derivatives (both spatial and temporal). As the discretisation is an approximation, it does not give a perfect solution and w tends to 'drift' during the simulation, especially when L^n is changed.

Luckily, as the pressure values are also calculated from derivatives of the velocity, the absolute states of v and w do not matter. The difference in values at the connection point is also irrelevant as there is no spatial derivative taken between v and w (refer to Figure 2). Finally, the pressure values are used for the sound-output of the simulation, so the drift does not cause any audible artefacts.

The absolute states do, however, need to be accounted for when adding points to the velocity vectors in (34). The current drift can be approximated by observing the difference between $w_{-1/2}^{n-1/2}$ and $v_{M+1/2}^{n-1/2}$, as these have approximately the same x location ($x_{w_{-1/2}}^n \approx x_{v_{M+1/2}}^n$) when a grid point is added. This is then used in a drift-correction vector $\boldsymbol{\eta}^{n-1/2}$ presented in (35). When a point is added to v, the values of w in $\mathbf{z}_v$ are offset by the aforementioned difference and when a point is added to w the same happens (inverted) for the values of v in $\mathbf{z}_w$. This way, the drift is allowed, but does not affect the state of the newly added grid points. Note that the drift does not affect the operations of point removal in (38).

4.4. State Correction

As L^n, and with that the number of grid points, is decreased, it might occur that the inner boundaries p_M^n and q_0^n have a very different value when $\alpha \gtrsim 0$, i.e., right before a point is removed. This violates the rigid connection in Eq. (28).

We propose in [6] to add an artificial spring-like connection between the inner boundaries that "corrects" the state of these points. Applying this to system (24) extends Eqs. (24a) and (24c) according to

$$\frac{\bar{S}_l}{\rho_0 c^2}\delta_{t+}p_{l_p}^n = -\delta_{x-}(S_{l+1/2}v_{l_p+1/2}^{n+1/2}) + J_p(x_{p_M})F_{\text{sc}} \tag{39a}$$

$$\frac{\bar{S}_l}{\rho_0 c^2}\delta_{t+}q_{l_q}^n = -\delta_{x+}(S_{l-1/2}w_{l_q-1/2}^{n+1/2}) - J_q(x_{q_0})F_{\text{sc}} \tag{39b}$$

where spreading operators

$$J_p(x_i) = \begin{cases} \frac{1}{h}, & l_p = l_{p,i} = \lfloor x_i/h \rfloor \\ 0, & \text{otherwise,} \end{cases} \quad \text{and}$$
$$J_q(x_i) = \begin{cases} \frac{1}{h}, & l_q = l_{q,i} = \lfloor x_i/h \rfloor - M \\ 0, & \text{otherwise,} \end{cases} \tag{40}$$

correction effect

$$F_{\text{sc}} = \beta\left(\omega_{\text{sc}}^2\mu_{t\cdot}\eta_{\text{sc}}^n + \sigma_{\text{sc}}\delta_{t\cdot}\eta_{\text{sc}}^n\right) \tag{41}$$

(in m^3/s)..units stop making sense here as this is an artificial connection "force".. might just exclude them?, with spring stiffness

ω_{sc}, spring damping σ_{sc}, pressure difference

$$\eta_{\text{sc}}^n \triangleq q_0^n - p_M^n \tag{42}$$

(in N/m^2) and scaling coefficient

$$\beta = \beta(\alpha) = \frac{1-\alpha}{\alpha+\epsilon}, \tag{43}$$

where $\epsilon \ll 1$ to prevent division by 0. Just like in [6], implementing the pressure difference allows for an infinite β ($\epsilon = 0$) acting like a rigid connection between Eqs. (39a) and (39b).

Matrix form here??

One can write the entire system above in matrix form by concatenating...

5. IMPLEMENTATION

This section provides some details on the implementation of the algorithm.

5.1. Parameters

For the most part, the parameters used in the simulation have been obtained from [10, 11, 12]. The lengths and radii of different parts of the tube can be found in Table 1 and a diagram showing this geometry is shown in Figure 3. The system is split at the end of the trombone slide such that the ranges for the lengths of the two tubes are $L_p^n \in [0.797, 1.327]$ and $L_q^n \in [1.796, 2.326]$.

Other parameters used in the simulation can be found in Table 2. Not included here, is λ which has been set slightly lower than the stability condition in (19), i.e., $\lambda = 0.9999$. Although the implementation works when $\lambda = 1$, this is done to tolerate (much) higher speeds of change in L^n before instability occurs (see Section 5.2). Not satisfying condition (19) causes bandlimiting and dispersive effects [13], but such a small deviation from the condition has no audible influence on the output sound and outweighs the problems caused by instability.

As the tube acts mainly as an amplifier for specific resonant frequencies it is important to match the frequency of the lip reed to a resonating mode of the tube (which depends on L^n). This is done according to

$$\omega_0^{n+1/2} = \mathcal{F}\frac{2\pi c}{\rho_0 L^{n+1/2}} \tag{44}$$

where $L^{n+1/2} = L^n$ and scalar multiplier $\mathcal{F} \approx 2.4$ double check this was heuristically found to best match the 4$^{\text{th}}$ resonating mode of the tube and generates a recognisable brass sound.

The output of the system can be retrieved by selecting a grid point on the pressure grid and listening to this at the given sample rate f_{s}. The most logical would be to listen to the rightmost grid point, i.e., the radiating boundary $q_{M_q}^n$ as this is also where the sound enters the listening space in the real world.

5.2. Limit on speed of change

To reduce audible artefacts and instability issues form adding and removing points also to stay in the sub-audio rate regime, a limit can be placed on (31) as

$$L_{\text{diff}}^n \leq \mathcal{N}_{\text{maxdiff}} h \tag{45}$$

Part of tube	Length (cm)	Radius (cm)
Inner slide (1)	70.8	0.69
Outer slide (extended) (2)	53	0.72
Slide crook (3)	17.7	0.74
Outer slide (extended) (4)	53	0.72
Inner slide (5)	71.1	0.69
Gooseneck (6)	24.1	0.71
Tuning slide (7)	25.4	0.75, 1.07
Bell flare (8)	50.2	1, 10.8

Table 1: Geometry of a measured trombone taken from [11]. Numbers correspond to Figure 3.

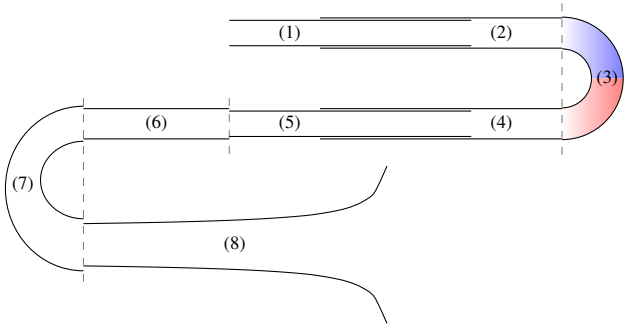

Figure 3: Diagram showing the trombone geometry (not to scale). Numbers correspond to the parts of the tube found in Table 1 and dashed lines highlight where the different parts are separated. The tube is split in the middle of the slide crook with the colours corresponding to those in 2.

where $\mathcal{N}_{\text{maxdiff}}$ is the maximum change in $\mathcal{N}$ per sample and has been set to $\mathcal{N}_{\text{maxdiff}} = 1/20$. This means that a grid point can be added or removed every 20 samples and allows the entire range of L to be traversed in ca. 0.06 s at a sample rate of $f_{\text{s}} = 44100$ Hz. still sub-audio rate?

5.3. State correction

The centred operators in Eq. (41) and with that the introduction of states at $n+1$ seem to make the scheme implicit. It is, however, possible to calculate F_{sc} explicitly [13, 14].

The the aforementioned operators also introduce the need for values at $n-1$, i.e., p_M^{n-1} and q_0^{n-1}. Therefore, the vectors $\mathbf{p}^{n-1}$ and $\mathbf{q}^{n-1}$ will need to be stored, and the operations to add and remove grid points as described in 4.2 need to be applied to these as well. One could argue that only two points at the inner boundaries are needed to create $\mathbf{r}^{n-1}$, but for generality, we continue with the entire vectors defined over the same domains as $\mathbf{p}^n$ and $\mathbf{q}^n$ respectively.

check centered and centred (both papers)

5.4. Real-time implementation

The algorithm has been implemented in C++ using the JUCE framework.

It might happen that the denominator in (22b) is zero, especially when the system has not been activated for a while. In this

Name	Symbol (unit)	Value
Tube		
Length	L (m)	$2.593 \leq L \leq 3.653^{\star}$
Air density	ρ_0 (kg/m^3)	1.1769**
Wave speed	c (m/s)	347.23**
Geometry	S (m^2)	See Table 1.
Lip reed		
Mass	M_r (kg)	$5.37 \cdot 10^{-5}$*
Frequency	ω_0 (rad/s)	$1194 \leq \omega_0 \leq 1683$
Mouth pressure	P_m (Pa)	$0 \leq P_\mathrm{m} \leq 6000$??
Damping	σ_r (s^{-1})	5*
Eff. surface area	S_r (m^2)	$1.46 \cdot 10^{-5}$*
Width	w_r (m)	0.01*
Equilibrium sep.	H_0 (m)	$2.9 \cdot 10^{-4}$*
Coll. stiffness	K_c (N/m)	10^4
Nonlin. coll. coeff.	α_c (-)	3
Miscellaneous		
Sample rate	f_s (Hz)	44100

Table 2: List of parameter values used for the simulation. Taken from *[11], *[10] or **[12] with temperature $T = 26.85^{\circ}C$.

case $g^{n+1/2}$ is set to 0 and (**??**) is not executed.

5.5. Order of Calculation

Algorithm 1 shows some pseudocode

while *application is running* **do**
  Retrieve new parameters (L^n, ω_0^n and P_m^n)
  Update L_p^n and L_q^n (Eqs. (31), (45) and (30))
  Calc. $\mathcal{N}^n$ and N^n (Eqs. (26) and (16))
  Calc. α (Eq. (27))
  if $N^n \neq N^{n-1}$ **then**
    Add or remove point (Eq. (34) or (38))
    Update M and M_q (Eq. (23))
  end
  Calc. p_{M+1}^n and q_{-1}^n (Eqs. (29))
  Calc. $\mathbf{v}^{n+1/2}$ and $\mathbf{w}^{n+1/2}$ (Eqs. (24b) and (24d))
  Calc. $y^{n+3/2}$ w/o collision (Eqs. (21))
  Calc $g^{n+1/2}$ (Eq. (22))
  Calc. $y^{n+3/2}$ with collision (Eqs. (21))
  Calc. U_B and U_r (Eqs. (21c) and (21d))
  Calc. $\mathbf{p}^{n+1}$ and $\mathbf{q}^{n+1}$ (Eqs. (39))
  Retrieve output
  Update system states ($\mathbf{p}^{n-1} = \mathbf{p}^n$, $\mathbf{p}^n = \mathbf{p}^{n+1}$)
  (same for $\mathbf{v}^{n-1/2} = \ldots$, $y^{n-1/2}$, $y^{n+1/2}$, and ψ^n),
  Update N ($N^{n-1} = N^n$)
  Increment n
end

Algorithm 1: Pseudocode showing the order of calculations of the algorithm implementing the trombone .

6. RESULTS AND DISCUSSION

Informal evaluation by the authors concluded that although the sound has brass-like qualities, it does not sound fully realistic. The model could be extended by adding viscothermal losses [15] or nonlinear effects [2].

The limit placed on the speed of change of L^n in (45) does not affect the feeling of real-time change when controlling the application.

The main difference with [6], is that the method is applied to a system of first-order equations rather than the second-order 1D wave equation.

As the geometry varies it matters a lot where points are added and removed as this might influence the way that the method is implemented. speculative section coming up The middle of the slide crook was chosen, both because it would be reasonable for the air on the tube to "go away from" or "go towards" that point as the slide is extended or contracted, and because the geometry does not vary there. Experiments with adding / removing grid points where the geometry varies have been left for future work. even more speculative.. → It could be argued that it makes more sense to add points at the ends of the inner slides as "tube material" is also added there. This would mean that the system should be split in three parts: "inner slide", "outer slide" and "rest", and would complicate things even more.

Experiments have been done with alternating between calculating the virtual grid points using the pressure and the velocity, where rather than adding points to the left and right system in alternating fashion, points were added to pressures p and q and velocities v and w respectively.

7. CONCLUSION AND FUTURE WORK

This paper presented a full implementation of the trombone using FDTD methods including a lip reed, bell-radiation and a tube discretised using a dynamic grid.

Investigate the possibility of adding / removing grid points at points where the cross-sectional area is varying.

8. ACKNOWLEDGEMENTS

This work is supported by NordForsk's Nordic University Hub Nordic Sound and Music Computing Network NordicSMC, project number 86892.

9. REFERENCES

[1] M. Campbell, "Brass instruments as we know them today," *Acta Acustica united with Acustica*, vol. 90, no. 4, pp. 600–610, 2004.

[2] R. Msallam, S. Dequidt, S. Tassart, and R. Causse, "Physical model of the trombone including non-linear propagation effects," in *ISMA: International Symposium of Music Acoustics*, 1997.

[3] R. Msallam, S. Dequidt, R. Causse, and S. Tassart, "Physical model of the trombone including nonlinear effects. application to the sound synthesis of loud tones," *Acta Acustica united with Acustica*, vol. 86, no. 4, pp. 725–736, 2000.

[4] P. R Cook, *Real sound synthesis for interactive applications*, CRC Press, 2002.

[5] R. L. Harrison, S. Bilbao, J. Perry, and T. Wishart, "An environment for physical modeling of articulated brass instruments," *Computer Music Journal*, vol. 39, no. 4, pp. 80–95, 2015.

[6] S. Willemsen, S. Bilbao, M. Ducceschi, and S. Serafin, "Dynamic grids for finite-difference schemes in musical instrument simulations," submitted to *Proc. of the 23rd Int. Conf. on Digital Audio Effects (DAFx)*, 2021.

[7] M. Ducceschi, S. Bilbao, S. Willemsen, and S. Serafin, "A non-iterative solver for collision dynamics based on energy quadratisation," accepted to *Journal of the Acoustical Society of America (JASA)*, 2021.

[8] H. Levine and J. Schwinger, "On the radiation of sound from an unflanged circular pipe," *Physical Review*, vol. 73, no. 2, pp. 383–406, 1948.

[9] F. Silva, P. Guillemain, J. Kergomard, B. Mallaroni, and A. Norris, "Approximation formulae for the acoustic radiation impedance of a cylindrical pipe," *Journal of Sound and Vibration*, vol. 322, pp. 255–263, 2009.

[10] R. L. Harrison-Harsley, *Physical Modelling of Brass Instruments using Finite-Difference Time-Domain Methods*, Ph.D. thesis, University of Edinburgh, 2018.

[11] T. Smyth and F. S. Scott, "Trombone synthesis by model and measurement," *EURASIP Journal on Advances in Signal Processing*, 2011.

[12] A. H. Benade, "On the propagation of sound waves in a cylindrical conduit," *Journal of the Acoustical Society of America*, vol. 44, no. 2, pp. 616–623, 1968.

[13] S. Bilbao, *Numerical Sound Synthesis*, John Wiley & Sons, United Kingdom, 2009.

[14] S. Bilbao, "A modular percussion synthesis environment," in *Proc. of the 12th Int. Conference on Digital Audio Effects (DAFx)*, 2009.

[15] S. Bilbao and R. L. Harrison, "Passive time-domain numerical models of viscothermal wave propagation in acoustic tubes of variable cross section," *The Journal of the Acoustical Society of America*, vol. 140, pp. 728–740, 2016.

[16] Tamara Smyth and Frederick S Scott, "Trombone synthesis by model and measurement," *EURASIP Journal on Advances in Signal Processing*, vol. 2011, pp. 1–13, 2011.

[17] JUCE, "JUCE," Available at https://juce.com/, accessed March 21, 2021.